AAPS PharmSciTech (2019) 20: 107
DOI: 10.1208/s12249-019-1310-6

Research Article

Theme: Lipid-Based Drug Delivery Strategies for Oral Drug Delivery
Guest Editor: Sanyog Jain

Lipopolysaccharide Polyelectrolyte Complex for Oral Delivery of an Anti-tubercular Drug

Mumuni Sumaila,[1] Poornima Ramburrun,[1] Pradeep Kumar,[1] Yahya E. Choonara,[1] and Viness Pillay[1,2]

Received 3 October 2018; accepted 10 January 2019; published online 11 February 2019

Abstract. Anti-tuberculosis drug delivery has remained a challenge due to inconsistent bioavailability and inadequate sustained-release properties leading to treatment failure. To resolve these drawbacks, a lipopolysaccharide polyelectrolyte complex (PEC) encapsulated with rifampicin (RIF) (as the model drug) was fabricated, using the solvent injection technique (SIT), with soy lecithin (SLCT), and low-molecular-weight chitosan (LWCT). The average particle size and surface charge of RIF-loaded PEC particulates was 151.6 nm and + 33.0 nm, respectively, with noted decreased particle size and surface charge following increase in SLCT-LWCT mass ratio. Encapsulation efficiency (%EE) and drug-loading capacity (%LC) was 64.25% and 5.84%, respectively. Increase in SLCT-LWCT mass ratio significantly increased %EE with a marginal reduction in %LC. *In vitro* release studies showed a sustained-release profile for the PEC particulate tablet over 24 h (11.4% cumulative release) where the dominant release mechanism involved non-Fickian anomalous transport shifting towards super case II release as SLCT ratios increased (6.4% cumulative release). PEC-tablets prepared without SIT presented with rapid Fickian-diffusion-based drug release with up to 90% RIF release within 4 h. *Ex vivo* permeability studies revealed that lipopolysaccharide PEComplexation significantly increased the permeability of RIF by ~ 2-fold within the 8-h study period. These results suggest successful encapsulation of RIF within a PEC structure while imparting increased amorphic regions, as indicated by x-ray diffraction, for potential benefits in improved drug dissolution, bioavailability, and dosing.

KEY WORDS: polyelectrolyte complexation; lipopolysaccharide; PEC particulates; tuberculosis; mucoadhesion; rifampicin.

INTRODUCTION

Tuberculosis (TB) has been a major public health challenge, particularly in Africa, Asia, and South America, despite all efforts made to improve its treatment and management (WHO 2017). Moreover, TB has been associated with high mortality rates, in co-morbid human immunodeficiency virus (HIV) incidences (1). The causative organism, *Mycobacterium tuberculosis* (MTB) primarily affects the lungs as pulmonary TB; however, other parts of the body could also be affected resulting in extrapulmonary TB (2). The conventional anti-TB regimen involves the oral administration of rifampicin, isoniazid, pyrazinamide or ethambutol in various combinations often dosed multiple times per day (1). Patients of this "hard to eradicate" bacteria (MTB) suffer severe adverse effects due to major drawbacks associated with the delivery of this chemotherapy regimen (3). The current TB therapeutic strategy is challenged with problems of low drug solubility, intestinal malabsorption, pre-mature drug degradation, low drug concentrations at the infection site, and poor cell-drug penetration (3). All these factors impart poor bioavailability of TB medications. Furthermore, the long (6–9 months) and stringent treatment schedule of anti-tubercular drugs (ATDs) and associated side-effect profiles (particularly the second-lines ATDs) contributes to poor patient compliance (4). These challenges necessitate action to develop an effective delivery system capable of alleviating these concerns. A nanocarrier system capable of releasing bioactives steadily in therapeutically effective quantities

Guest Editor: Sanyog Jain

Mumuni Sumaila and Poornima Ramburrun contributed equally to the research.

[1] Wits Advanced Drug Delivery Platform Research Unit, Department of Pharmacy and Pharmacology, School of Therapeutic Sciences, Faculty of Health Sciences, University of the Witwatersrand, Johannesburg, 2193, South Africa.
[2] To whom correspondence should be addressed. (e–mail: viness.pillay@wits.ac.za)

could assist in improving drug target-site bioavailability, cell-drug penetration, intestinal absorption, and protection against pre-mature drug degradation while reducing the dosage frequency of the medication thereby improving patient compliance.

In the quest for solutions to the aforementioned challenges, several studies have successfully fabricated nanodelivery systems to efficiently deliver ATDs. Some of which include hybridized lipid-polymer systems (5,6), liposomal systems (7,8), natural polymeric systems (9,10), synthetic polymeric systems (11,12) and systems for localized lung delivery (13,14). Formulations with synthetic polymers face some drawbacks as regards to safety and biocompatibility. Likewise, inhalational and intravenous formulations may be less cost-effective and administration and ease of use could pose a challenge to the patient. Lipopolysaccharide-based polyelectrolyte complex (PEC) particulates would be an excellent drug delivery strategy for the smart delivery of ATDs *via* the conventional oral route through the elimination of initial burst release and improvement of drug solubility and permeability which are not consistently attainable with nanoemulsions, polymeric, and non-polymeric nanoparticles and polymeric micelle nanocarriers (3). The composition of such a system as a polymeric complex combines the advantages of a biodegradable polysaccharide (for structural integrity, physical stability, and bioactive protection) (15,16) and phospholipid (for high drug-loading capacity and sustained release). In addition, lipopolysaccharide-based PEC particulates offer the advantages of improved biocompatibility, versatility, safety, and efficacy (17,18) with relatively cost-effective naturally derived polymers.

Low-molecular-weight chitosan (LWCT) is a deacetylated linear polysaccharide represented by (1-4)-2-amino-2-deoxy-B-D-glucan. This copolymer of glucosamine and N-acetylglucosamine with a positive surface charge (19) contributes to its reactive ability to form PECs with anionic molecules (20). Soy lecithin (SLCT) in contrast, a negatively charged polymer with a high complexation affinity for LWCT, has gained much attention for the synthesis of solid-lipid nanoparticles, micro- and nano-emulsions, and liposomes (7).

To the best of our knowledge, there have been no reports of a lecithin-chitosan nanodelivery system specifically designed for oral delivery of rifampicin. However, several studies have investigated similar systems, with favorable outcomes, in cancer chemotherapy (21), transdermal melatonin delivery (22), and oral insulin delivery (23). Likewise, the formulation in the present study is based on the PEC that occurs between the free anionic phosphate group of the phospholipid (SLCT) and the free cationic amine group of the polysaccharide (LWCT). Polyelectrolyte complexation is a self-sustaining reaction which does not require further reaction initiators, catalysts, or cross-linkers. In addition, the popularized use of cost-effective naturally derived polymeric materials for the synthesis of drug-delivery systems propose reliable safety and non-toxicity as a result of an ecologically positive tactic and non-complex formulation procedure (24,25). Of particular importance to this study is the notion that varying degrees of polyelectrolyte complexation enhances drug bioavailability (26), improves drug encapsulation efficiency, and influences drug-release kinetics of nanoparticulate formulations (27).

The present study aims to fabricate a lipopolysaccharide-based PEC particulates for application as a sustained-release oral delivery system for ATDs with the goal of improving patient compliance and therapeutic efficacy with regard to bioavailability. This study incorporated LWCT and SLCT for the polyelectrolyte complex using the solvent injection technique with rifampicin (RIF) as the model drug. The synthesized RIF-loaded PEC particulates were analyzed for molecular and crystallinity transitions to establish polyelectrolyte complexation with subsequent characterization of rheological properties, formulation stability, and light scattering behavior of the nanoparticle suspension, mucoadhesion, thermodynamic and hydrodynamic properties, permeability, and drug release studies. To effectively study the drug release profile of the fabricated particulates as a function of the PEC, a 4 × 2 matrix system was implemented: (1) PEC particulates of interest with encapsulated RIF (SLCT-LWCT-RIF), (2) *in situ* mixing of RIF with the formulated SLCT-LWCT+RIF complex (where RIF is not encapsulated), (3) *in situ* complex of pristine SLCT+LWCT+RIF, and (4) *in situ* complex of SLCT-coated RIF and pristine LWCT (MSLCT+RIF+LWCT). Furthermore, mathematical modeling of the drug release kinetics was performed to elucidate insight into the drug release mechanisms acting upon the various formulations.

MATERIALS AND METHODS

Materials

LWCT (75–85% deacetylated), L-α-lecithin soybean (a concentrate of soybean lecithin with 94% phosphatidylcholine and < 2% triglycerides), porcine mucin (PM) (type 2), RIF, and phosphate-buffered solution (PBS) were purchased from Sigma-Aldrich (St. Louis, MO, USA). Ethanol (ETOH) and glacial acetic acid were procured from Merck (Pty Ltd., South Africa). All chemicals were of analytical reagent grade and used without prior modification. Double deionized water (DDW) was used for all the preparations.

Preparation of Rifampicin-Loaded SLCT-LWCT Lipopolysaccharide Particulates

Preparation of Loose Nanoparticle Powders

Lipopolysaccharide PEC particulates were prepared using an adapted solvent injection technique (as shown in Fig. 1) from Sonvico and co-workers(28). Briefly, 300 mg of SLCT was dissolved in 10 mL of ethanol followed by an addition of 150 mg RIF which was thoroughly dissolved to obtain a homogenous SLCT-RIF solution. LWCT solution was prepared by dissolving 100 mg polymer in 40 mL of a 1% *v/v* acetic acid solution and 50 mL DDW. The RIF-loaded nanoparticle suspension of a 3:1 SLCT-LWCT weight ratio was obtained by injecting 10 mL of SLCT-RIF ethanol solution (30 mg/mL) into 90 mL of LWCT solution through a syringe (inner diameter 0.75 mm, flow

rate 40 mL/min) with subsequent mechanical stirring. The resulting nanoparticle suspension was centrifuged at 5000 rpm for 30 min, the supernatant decanted, and sediment lyophilized to obtain a dried nanoparticle powder. The same procedure was followed for the preparation of PEC particulates of a 1:1 SLCT-LWCT weight ratio and RIF-free formulation.

Preparation of PEC Particulate Tablets

For simplicity of sample preparation for the determination of *in vitro* drug release profiles, textural profiling, and hydration dynamics, the resulting dried nanoparticle powders were compressed into tablets. Batches of nanoparticle powder (SLCT-LWCT-RIF 1:1 and 3:1) containing 300 mg RIF was compressed into tablets using a die punch fitted into a hydraulic unit model tablet press machine (Carver, Inc. Wabash, USA) under an applied pressure of 1400 psi. The preparation of SLCT-LWCT+RIF tablets involved the mixing of RIF with preformulated SLCT-LWCT complex. For the preparation of SLCT+LWCT+RIF tablets, pristine polymers and RIF (300 mg SLCT + 300 mg LWCT + 300 mg RIF) were mixed together before punching. The preparation of MSLCT+RIF+LWCT tablets required melting of 300 mg SLCT at 45°C which was then subsequently used to coat 300 mg RIF. Thereafter, SLCT-coated RIF was mixed with 300 mg pristine LWCT and then punched into tablets.

Evaluation of Particle Size Distribution, Zeta Potential, and Conductivity

Briefly, 100 mg of the synthesized PEC particulates were dispersed in DDW and sonicated for 30 s. A 2-mL sample of the nanoparticle suspension was placed in disposable cuvettes and analyzed at 25°C for average particle size, polydispersity index (PDI), zeta potential, and conductivity using the Malvern ZetaSizer Nano ZS (Malvern Instruments, Worcestershire, UK).

Determination of RIF-Loading Capacity and Encapsulation Efficiency in Response to Changes in SLCT Concentration

Drug-loaded nanoparticle suspensions (2 mL; $n = 3$), were centrifuged at 5000 rpm for 1 h. The concentration of RIF in the clear supernatant was analyzed by UV-Vis spectroscopy (Specord40, Analytik Jena, AG, Germany) set at $\lambda_{max} = 475$ nm. Triplicate measurements were carried out to determine the %encapsulation efficiency (%EE) and %drug-loading capacity (%LC) of the PEC particulates using Eqs. (1) and (2), respectively:

$$\%EE = \frac{\text{Total amount of RIF loaded} - \text{Amount of RIF in the supernatant}}{\text{Total amount of RIF loaded}} \times 100 \quad (1)$$

$$\%LC = \frac{\text{Amount of RIF in PEC particulates}}{\text{Weight of PEC particulates}} \times 100 \quad (2)$$

Determination of mucoadhesive properties in response to SLCT/LWCT and RIF variations

In vitro mucoadhesion analysis was performed using PM to determine %mucin-binding efficiency (%MBE) to confirm interactions between the PEC particulates and PM with regard to the effect of RIF loading on the mucoadhesive property of the PEC particulates (29). Briefly, 2-mL samples of nanoparticle suspension (0.5 mg/mL) was mixed with 2 mL of PM (1 mg/mL) solution prepared in phosphate-buffered saline (PBS) (pH 6.8). This colloidal mixture was incubated at 37°C for 2 h in an incubation chamber with a rotation of 20–25 rpm. Thereafter, the sample was centrifuged at 5000 rpm for 30 min and the absorbance of the supernatant measured at $\lambda_{max} = 250$ nm by UV-Vis spectroscopy. Triplicate measurements were performed and %MBE of the various nanoparticle formulations calculated using Eq. (3):

$$\%MBE = \frac{C_i - C_p}{C_i} \times 100 \quad (3)$$

where C_i is the original PM concentration used for incubation and C_p is the concentration of free PM in the supernatant.

Determination of Molecular Vibrational Transitions and Analysis of PEC Formation

Powdered samples of RIF-loaded and RIF-free SLCT-LWCT PEC particulates and the native polymers were analyzed for interactions resultant of PEC formation. Samples were analyzed at a resolution of 4 cm^{-1} over a wavelength range of 4000 cm^{-1} to 650 cm^{-1} using the PerkinElmer Spectrum 2000 ATR-FTIR (PerkinElmer 100, Llantrisant, Wales, UK).

Analysis of the Thermodynamic Properties of the Synthesized Lipopolysaccharide PEC and RIF-Loaded PEC Particulates

The thermodynamic properties of the SLCT-LWCT PEC, SLCT-LWCT-RIF PEC particulates and the pristine constituent polymers and drug were evaluated using a temperature modulated differential scanning calorimeter (TMDSC) (Mettler Toledo, DSC, STAReSystem, Swchwerzenback, ZH, Switzerland). Samples of 5–10 mg were sealed in aluminum crucibles and heated over a 10–325°C temperature range at a heating rate of 5°C/min under continuous flow of nitrogen gas at 200 mL/min. The DSC thermograms were obtained as plots of heat flow against sample temperature.

X-ray Powder Diffraction Analysis

The crystallinity transitions of the RIF-loaded PEC particulates, RIF-free SLCT-LWCT complex, and native polymers were analyzed using x-ray powder diffraction (XRPD) (Rigaku MiniFlex 600, Tokyo, Japan) sourced with nickel-filtered CuKα radiation (at a voltage of 40 kV and a current of 15 mA). Diffractograms were obtained using a 2θ scan range over 3–80° at a scanning rate of 5° per minute.

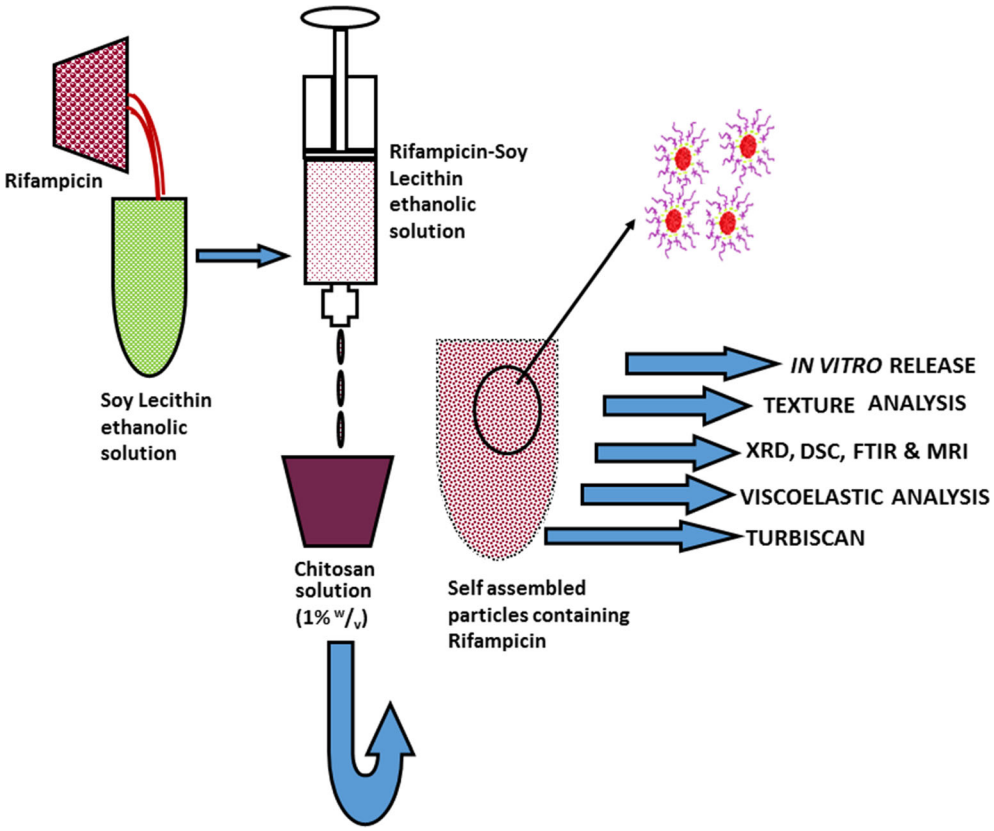

Fig. 1. Schematic representation of the synthesis of lipopolysaccharide-based PEC particulates *via* the solvent injection technique

Evaluation of Rheological Properties of the Synthesized Lipopolysaccharide Complex and RIF-loaded PEC Particulates

The kinetic gelation properties of the PEC formulations were analyzed using the ElastoSens™ Bio^2 (Rheolution Instruments, Canada) which employed a non-destructive acoustic vibration and laser measurement of rheological responses without sample contact (30). Samples were studied by mixing appropriate volumes of 0.1% *w/v* SLCT and 0.1% *w/v* LWCT solutions (in SLCT-LWCT ratios of 1:1 and 3:1) in the sample holder where polyelectrolyte complexation reactions were allowed to occur at 37°C over a 5-h duration. The experimental procedure was repeated for the incorporation of RIF into the reaction system (polymer complex/RIF ratio of 5:1). The same solvents, as mentioned earlier, were used for preparation of the polymer solutions. The shear storage modulus G' (Pa) was obtained as a function of time (s).

Textural Profiling of RIF-loaded Lipopolysaccharide Complex Nanoparticle Tableted Formulations

Textural profiling, in terms of matrix breakpoint (N) and fracture energy (N.mm), of the SLCT-LWCT-RIF 1:1 and 3:1 tablets was performed using a texture analyzer (TA.*XTplus*, Stable Microsystems, Surrey, UK) fitted with a flat-tipped stainless steel probe of 2 mm in diameter. The test parameters consisted of a pre-test and test speed of 2 mm/s, post-test speed of 10 mm/s, and an Auto-type trigger force of 0.05 N with a 5 kg load-cell. The maximum peak point and area under the curve of the force-distance textural profile allowed the determination of the force at matrix breakpoint and corresponding fracture energy.

Optical Characterization and Stability of the Lipopolysaccharide PEC Particulates in Suspension

Optical interactions and formulation stability of the formulated nanoparticle suspensions were investigated utilizing the Turbiscan™ LAB (Formulaction, L'Union, France). A 20-mL aliquot of RIF-loaded and RIF-free nanoparticle suspensions were introduced into specialized sample holders and analyzed at pre-determined intervals over a 5-min duration at 25 (± 0.5)°C. The instrument was fixed with a pulsed near infrared light source moving vertically along the sample collecting data at 40-μm intervals. A 180° positioned transmission detector detected transmitted light whereas a backscattering detector, positioned at 45°, detected rebounded light in response to the light-scattering effect by the suspended PEC particulates. The changes in backscatter (ΔBS) measurements were used to assess formulation stability.

In vitro Drug Release of Lipopolysaccharide PEC Particulates and Kinetic Modeling of Release Data

RIF-loaded nanoparticle tablets (SLCT-LWCT ratios of 1:1 and 3:1) containing 300 mg RIF were placed into vessels containing 900 mL of PBS pH 6.8 at 37°C in a dissolution tester (ERWEKA, USP Apparatus II, DT 126, UK) operated

at a paddle revolution of 50 rpm over a 24-h period. Samples of 5 mL of dissolution medium were withdrawn at predetermined time intervals and replaced with equal amounts of fresh PBS (pH 6.8) to maintain sink conditions. The RIF content in each sample was quantified using UV-Vis spectroscopy set at $\lambda_{max} = 475$ nm. The comparator formulations studied include (1) *in situ* mixing of RIF with the formulated SLCT-LWCT complex (SLCT-LWCT+RIF), (2) *in situ* complex of pristine SLCT+LWCT+RIF, (3) *in situ* complex of SLCT-coated RIF and pristine LWCT (MSLCT+RIF+LWCT), and (4) capsulated free RIF. Experimental data were obtained in triplicate and all values are representative of mean ± SD ($n = 3$). The release kinetics of RIF from the formulated nanoparticle-based tablets and comparator formulations were fitted into the zero-order (Eq. 4), first-order (Eq. 5), Higuchi (Eq. 6), Korsmeyer-Peppas (Eq. 7), and Hixson-Crowell (Eq. 8) kinetic models to assist in the elucidation of the primary drug release mechanisms (27).

$$C = K_0 t \tag{4}$$

where K_0 is the zero-order release constant at time t.

$$\mathrm{Log}C = \log C_0 - Kt/2.303 \tag{5}$$

where C_0 is the initial drug concentration and K is the first-order rate constant at time t.

$$Q = Kt^{1/2} \tag{6}$$

where Q reflects percent drug release and K is the design variable of the system at time t.

$$Q_0^{1/3} - Q_t^{1/3} = K_{HC} t \tag{7}$$

where Q_0 is the initial quantity of drug in the formulations, Q_t is the residual quantity of RIF at time t and K_{HC} is the rate constant.

$$M_t/M_\infty = Kt^n \tag{8}$$

where M_t/M_∞ is the fractional drug release at time t, K is the release rate constant, and n is the release exponent.

Analysis of the Hydrodynamic and Swelling Characteristics of the RIF-loaded Lipopolysaccharide PEC Tableted PEC Particulates

Analysis of the *in vitro* hydrodynamic and swelling behavior of the SLCT-LWCT-RIF nanoparticulate tableted formulation was performed *via* magnetic resonance imaging (MRI) (Oxford Instruments Magnetic Resonance, Oxon, UK) equipped with a 0.5 Tesla permanent magnet stabilized at 37°C and a dissolution flow-through cell containing PBS pH 6.8. Live-image capture of the SLCT-LWCT-RIF 1:1 and 3:1 tablets were obtained at 10-min intervals over a period of 16 h, respectively, utilizing MARAN-i Version 1.0 software.

Ex vivo Permeability of RIF from the Lipopolysaccharide PEC Particulates across Porcine Intestinal Tissue

Ex vivo permeability studies were performed, using static Franz Diffusion Cell Apparatus (Logan Instruments Corp., NJ, USA), to evaluate the permeability of RIF from the formulated PEC particulate systems (SLCT-LWCT-RIF 1:1 and SLCT-LWCT-RIF 3:1) and the free RIF across adult porcine intestinal epithelium of the large white pig. According to standard operating procedures and approval from the Animal Ethics Screening Committee of the University of the Witwatersrand (Clearance No. AESC-2014/38/C and Ref. 14-11-14 O), the pig was euthanized and the intestinal tissue was excised, cleaned and separated from the serosa then stored in PBS pH 6.8 until further use. Within 60 min of harvesting, the intestinal tissue was assessed for viability and integrity *via* potential difference measurements across the tissue sections using a Seven Multi GmbH S40 electrical conductivity meter (Mettler-Toledo, Zurich, Switzerland), over 8 h. Thereafter, the tissues were fixed between the donor and receptor compartments of the diffusion cells (permeation area 1.77 cm^2). The receptor chamber solution consisted of 12 mL PBS (pH 6.8), was continuously stirred with a magnetic bar and maintained at 37°C. The donor chamber consisted of 3 mL of the lipopolysaccharide PEC particulate dispersion containing 1.25 mg/mL of RIF. Samples of 3 mL were withdrawn from the receptor compartment at predetermined time intervals over 8 h and replaced with an equal volume of fresh PBS (pH 6.8) to maintain sink conditions. The samples were measured for the quantity of RIF using UV-Vis spectroscopy set at $\lambda_{max} = 475$ nm. Equations (9) and (10) were used to determine the quantity and flux of RIF, respectively, that traversed the intestinal tissue and Eq. (11) was used to determine permeation. Experimental data were obtained in triplicate and all values are representative of mean ± SD ($n = 3$).

$$\text{Cumulative amount of RIF permeated} = \frac{Q}{A}\left(\mathrm{mg/cm^2}\right) \tag{9}$$

where A is area of exposed membrane (cm^2) and Q is quantity of RIF crossing the membrane (mg).

$$J = \frac{\mathrm{Q}}{\mathrm{AT}}\left(\mathrm{mg/cm^2/min}\right) \tag{10}$$

where J is the flux of RIF, Q is the quantity of RIF permeated, A is the cross-sectional area of the membrane, and T is the time of exposure expressed in minutes.

$$-\ln\left(1 - \frac{2C_T}{C_0}\right) = \frac{2A}{V} \times P \times T \tag{11}$$

where C_T is the concentration of RIF in the receptor chamber at time T, C_0 is the original concentration of RIF in the donor chamber, V is the volume of solution in the two compartments, and A is the area of permeation.

RESULTS AND DISCUSSION

Evaluation of Particle Size and Zeta Potential

The average hydrodynamic diameters of the fabricated bioactive-loaded and empty PEC particulates as obtained from the Zetasizer® Nano-ZS were found to be in the range of 151.6 to 292.1 nm with a polydispersity index (PDI) of less than 0.3, as shown in Table I. The low PDI reveals a very narrow size distribution which is considered acceptable for an ideal nanoparticle (31). Furthermore, the obtained size range may indicate enhanced permeation of the PEC particulates across the intestinal mucosa thereby allowing for higher systemic levels of the formulation (32, 33). The average zeta potential of all the nano-suspensions ranged from + 22.2 to + 33.0 mV revealing the stability of the nano-suspension (34) in respect to coagulation, flocculation, aggregation, sedimentation, and creaming phenomena through strong electrostatic repulsion between the charged particles keeping them apart.

Determination of RIF-loading Capacity and Encapsulation Efficiency in Response to Changes in SlCT Concentrations

Determination of the drug-loading capacity (%LC) and encapsulation efficiency (%EE) of the lipopolysaccharide system (as shown in Table II) revealed that the 3:1 SLCT-LWCT PEC particulates achieved increased RIF drug-loading (73.21%) compared to the 1:1 system (64.25%). This could be attributed to hydrophobic interactions and association of RIF with the SLCT lipid bilayer architecture (35). A similar observation was noted by Were and co-workers, who reported increased drug encapsulation with increased phosphatidylcholine concentration (36), thereby, inferring that drug encapsulation may be tuned to the preferred dose by adjusting SLCT concentration (37).

Determination of Mucoadhesive Properties in Response to SLCT/LWCT and RIF Variations

Mucoadhesion is thought to be the ability of polymeric materials to adsorb onto the surface mucous of mucosal membranes (38), thereby lengthening the resident time of these materials at the target site. Furthermore, mucoadhesion allows permeation of mucoadhesive nanocarriers into the mucosal layer thereby potentiating an increase in absorption and bioavailability (39). In this regard, the mucoadhesive property of LWCT could enhance the oral delivery of RIF. Surface interactions between mucoadhesive polymers and the mucosal membrane has been identified to be either ionic, covalent, hydrophobic or physical in nature (40).

Table II. Encapsulation Efficiency and Loading Capacity of RIF-loaded and RIF-free Nanoparticle Formulations

Formulation	%EE	%LC
SLCT-LWCT 1:1	–	–
SLCT-LWCT 3:1	–	–
SLCT-LWCT-RIF 1:1	64.25	5.84
SLCT-LWCT-RIF 3:1	73.21	5.10

RIF rifampicin, *%EE* encapsulation efficiency, *%LC* loading capacity, *SLCT* soy lecithin, *LWCT* low-molecular-weight chitosan

Studies on the *in vitro* interaction of the RIF-loaded and RIF-free PEC particulates using PM indicated the mucoadhesion propensity of LWCT. As shown in Table III and Fig. 2, all the formulations reached equilibrium adsorption at 120 min following immersion in mucin solution. Mucoadhesive studies revealed a %MBE of more than 10% (14–30%) for all the nanoparticle formulations except SLCT-LWCT-RIF (3:1) which demonstrated a %MBE of 8.25%. This is most likely attributed to the low amount of LWCT in this formulation in ratio to SLCT. Furthermore, it was observed that RIF-loading and increased SLCT concentration caused a decrease in %MBE, hence, demonstrating that only LWCT imparts the mucin-binding property of the complex system. As noted in Fig. 3a, of the FTIR spectra, RIF encapsulation into the SLCT-LWCT system imparted a decreased intensity of the peak corresponding to the amino groups of LWCT. This could be explained by the spontaneous binding of RIF molecules to amino groups of LWCT thereby resulting in a reduced availability of free LWCT amino sites for interaction and subsequent binding with mucin. These interactions ascribe the decreased %MBE noted upon RIF encapsulation. This implies that increased availability of LWCT surfaces for mucin interaction and subsequent adsorption produces an expected increase in the %MBE of the nanoparticulate complex system. The mechanism of mucoadhesion is likely a result of ionic interaction between cationic LWCT and anionic mucous to produce ionic bonding.

Analysis of Molecular Vibrational Transitions Indicating PEC Formation

FTIR spectra of the native polymers, SLCT-LWCT complex and SLCT-LWCT-RIF PEC particulates are illustrated in Fig. 3. FTIR for pristine LWCT (Fig. 3d) showed

Table I. Particle Size, Zeta Potential, Conductivity, and PDI of RIF-loaded and RIF-free Nanoparticle Formulations

Formulation	Particle size (nm)	Surface charge (mV)	Conductivity (mS/cm)	PDI
SLCT-LWCT 1:1	292.1	+ 25.6	0.194	0.292
SLCT-LWCT 3:1	232.8	+ 22.2	0.081	0.273
SLCT-LWCT-RIF 1:1	151.6	+ 33.0	0.102	0.247
SLCT-LWCT-RIF 3:1	274.2	+ 30.7	0.057	0.262

PDI polydispersity index, *RIF* rifampicin, *SLCT* soy lecithin, *LWCT* low-molecular-weight chitosan

Table III. %MBE Comparison of RIF-loaded and RIF-free Nanoparticle Formulations as a function of Time

Time (min)	SLCT-LWCT 1:1	SLCT-LWCT 3:1	SLCT-LWCT-RIF 1:1	SLCT-LWCT-RIF 3:1
30	6.12	3.99	1.23	0.88
60	14.40	9.47	4.12	2.00
90	21.60	16.57	9.00	5.81
120	29.77	25.02	14.10	8.25
150	29.56	25.14	14.22	8.31
300	29.63	25.09	14.14	8.29

MBE mucin-binding efficiency, *RIF* rifampicin, *LWCT* low-molecular-weight chitosan, *SLCT* soy lecithin

characteristic peaks at wavenumbers 3284 cm^{-1}, 1375 cm^{-1}, and 1023 cm^{-1} which corresponded to N–H, C–N, and C–O stretching of the amide, respectively, while the peak at 1583 cm^{-1} indicated N–H bending. For pristine SLCT (Fig. 3e), noted peaks at 3011 cm^{-1}, 1726 cm^{-1}, and 1378 cm^{-1} were assigned to O–H, C=O, and P=O vibrations, respectively (41). A critical observation of the spectrum of SLCT-LWCT (Fig. 3b) complex in comparison with the native polymers, indicated that similar bands for C=O, C–N, and P=O exist at wavenumbers 1736 cm^{-1}, 1375 cm^{-1}, and 1241 cm^{-1}, respectively (41). It is noted that the band corresponding to the P=O vibration of SLCT has shifted to a lower wavenumber, thus, indicating electrostatic interaction and possible complexation with the amide groups of LWCT. The N–H stretching vibration of the RIF-loaded complex (Fig. 3a) shifted to a lower wavenumber of 3253 cm^{-1} with a P–O–C vibration peak observed at 988 cm^{-1}. These shifts may further suggest PEC formation occurring between the phospholipid (SLCT) and LWCT which originates from the interaction between the amino groups (NH^{3+}) of chitosan and the phosphate groups (PO^{3-}) of the phospholipid resulting in an aminophosphate-functionalized system.

The FTIR spectrum of RIF (Fig. 3c) shows characteristic peaks at 2938 cm^{-1} (C–H stretching), 1732 cm^{-1} (–C=O acetyl stretching), 1650 cm^{-1} (–C=N asymmetric stretching), 1569 cm^{-1} (C=C stretching), 1373 cm^{-1} (C-N stretching), and 1254 cm^{-1} (–C–O–C–ether group) (42). Similar bands were demonstrated by the RIF-loaded nanoparticle spectrum: C–H stretching, –C=O acetyl stretching, and C–N stretching at 2923 cm^{-1}, 1735 cm^{-1}, and 1377 cm^{-1}, respectively (5), hence, suggesting RIF encapsulation. The encapsulation of RIF into the polymeric complex induced structural changes as noted on the spectrum of RIF-loaded PEC particulates when compared to the drug-free PEC particulates. A noticeable increase in peak intensity is evident from bands 2923 cm^{-1} to 968 cm^{-1} in the SLCT-LWCT-RIF spectrum when compared to the RIF-free nanoparticle spectrum. This further confirms the successful loading of RIF into the system; however, it may suggest that RIF could have interfered with or obscured the NH^{3+} and PO^{3-} PEC reaction sites (43).

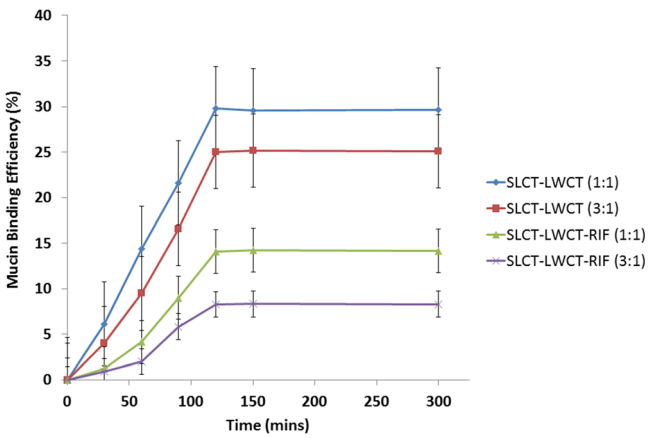

Fig. 2. Representation of %MBE of RIF-loaded and RIF-free nanoparticle formulations in response to SLCT/LWCT and RIF variations. All values represented as mean ± SD ($n = 3$)

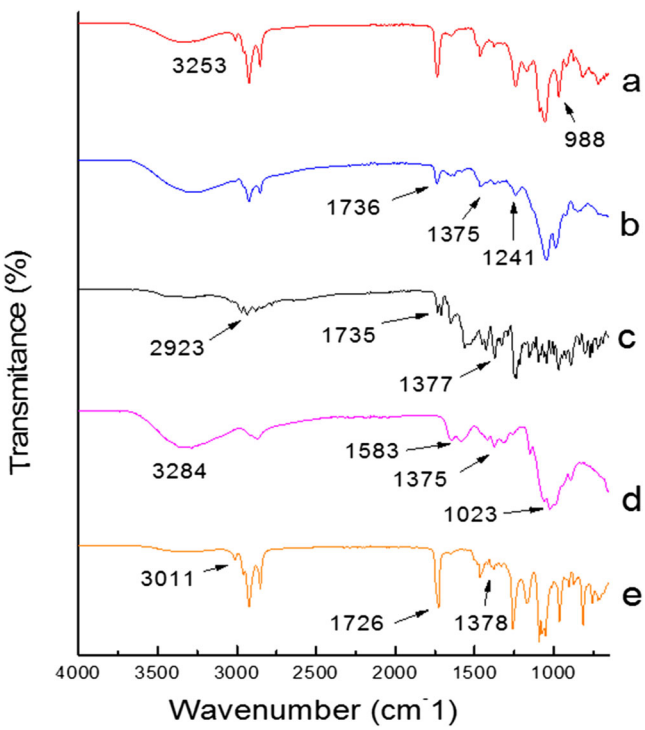

Fig. 3. FTIR spectra of **a** SLCT-LWCT-RIF, **b** SLCT-LWCT, **c** RIF, **d** LWCT, and **e** SLCT

Analysis of Thermal Stability and Degradation Induced by SLCT-LWCT-RIF Polyelectrolyte Complexation

DSC analysis, depicted in Fig. 4, allowed the elucidation of transitions in melting points and thermal degradation in response to variations of SLCT ratios and RIF encapsulation. Although no significant changes were noted in the thermal properties of RIF-loaded and RIF-free formulations, the formation of a PEC induced shifts of the degradation peaks towards higher temperatures. It is noted that formulations SLCT-LWCT-RIF 3:1 and 1:1 (Fig. 4a, b, respectively) and the corresponding RIF-free SLCT-LWCT 3:1 and 1:1 (Fig. 4c, d, respectively) PEC formulations exhibited the onset and endset of thermal degradation between a range of 288°C and 325°C, respectively, whereas the pristine LWCT (Fig. 4e) and SLCT (Fig. 4f) parent polymers exhibited lower thermal stability with the initiation of degradation occurring at 275°C. The thermogram of SLCT (Fig. 4f) presented with two melting points at 146°C and 222°C. The melting point at 222°C is observed to maintain its presence in the RIF-free and RIF-loaded formulations with a gradual shift of this peak towards higher temperatures where a marked increase to 242°C in the SLCT-LWCT-RIF 3:1 formulation is noted. These changes further confirm the formation of a PEC resulting from interaction of phosphate ions present in SLCT with the amines of LCWT. The melting point of pure RIF as noted at 187°C (Fig. 4g) is undetectable in the RIF-loaded formulations which may be attributed to the formation of a stable drug-polymer complex which necessitates higher energy to cause disruption of any newly formed chemical bonds.

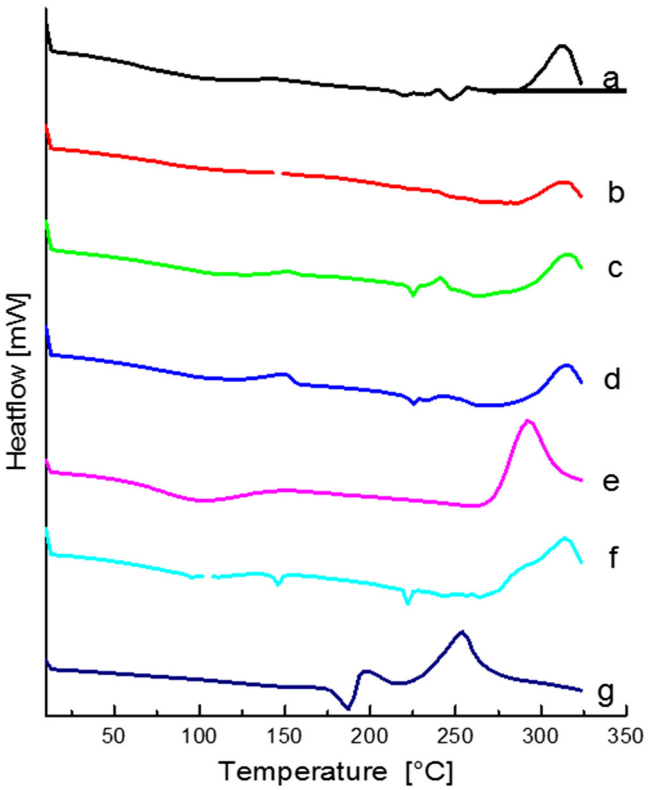

Fig. 4. DSC thermograms of **a** SLCT-LWCT-RIF 3:1, **b** SLCT-LWCT-RIF 1:1, **c** SLCT-LWCT 3:1, **d** SLCT-LWCT 1:1, **e** LWCT, **f** SLCT, and **g** RIF

XRPD Analysis

Crystallinity transitions of polymeric materials impact the resulting physicochemical properties. Amorphous characteristics of polymeric materials and colloid and emulsion systems are preferred for biomedical applications, especially in pharmaceutical industry, since the improved solubility of amorphous states enhance bioavailability (44). XRPD analysis performed for comparison between the characteristic crystalline properties of the pure RIF drug, native polymers, SLCT-LWCT complex and the RIF-loaded PEC particulates, as shown in Fig. 5. The XRPD pattern of pure chitosan, in a relatively amorphous state, has been reported to show broad peaks at $2\theta = 10°$ and $2\theta = 20°$ (45), which corresponds to the pattern obtained for pristine LWCT. The x-ray diffractogram of SLCT presented a semi-crystalline peak at $2\theta = 20.3°$ indicating the amorphous regions of phosphatidylcholine (46, 47). A comparison of the characteristic peaks evident in the native polymers with that of the new complex (SLCT-LWCT) formed revealed that the amorphous peak of pristine LWCT at $2\theta = 10°$ was absent in the formed SLCT-LWCT complex. Furthermore, the semi-crystalline peak of SLCT at $2\theta = 20.3°$ transitioned to a single strong and broad peak indicative of amorphous regions in the SLCT-LWCT and SLCT-LWCT-RIF complexes. These changes in crystallinity may be attributed to the polyelectrolyte complexation between NH^{3+} of LWCT and PO^{3-} of SLCT as described in FTIR spectra. RIF displayed well-defined narrow peaks characteristic of a highly crystalline structure. However, when encapsulated in the PEC particulates, the intense crystalline peak disappeared to form a combined singular broad peak, as depicted by the SLCT-LWCT-RIF diffractogram in Fig. 5. It was observed that the XRPD pattern for the RIF-loaded

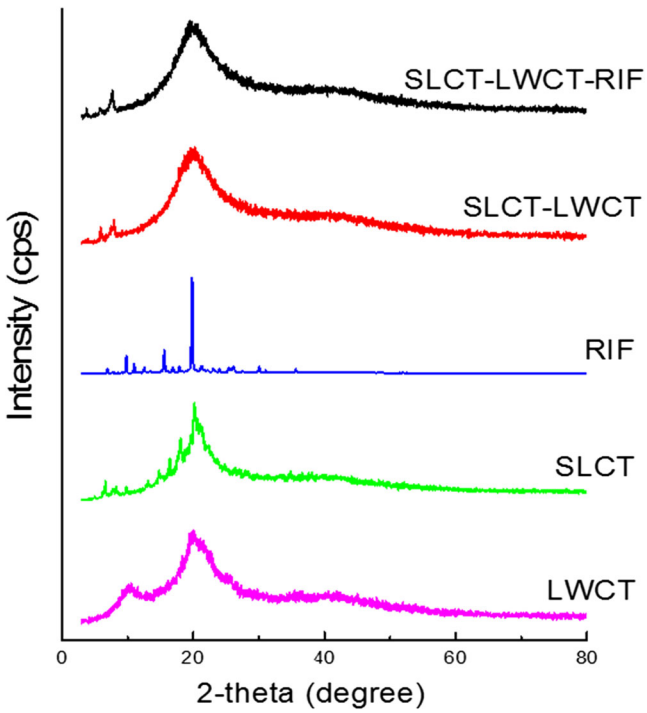

Fig. 5. X-ray powder diffraction (XPRD) spectra of LWCT, SLCT, RIF, the SLCT-LWCT complex, and the SLCT-LWCT-RIF PEC particulates

system and the RIF-free system showed marked similarity which may be attributed to the relatively small amount of RIF in terms of the drug/polymer complex ratio (1:40). However, maintenance of the presented amorphous regions in the RIF-loaded SLCT-LWCT complex may suggest an improved solubility profile of the encapsulated drug in aqueous media.

Evaluation of Rheological Properties of the Synthesized Lipopolysaccharide Complex and RIF-loaded PEC Particulates

Viscoelasticity studies with regard to the gelation kinetics and real-time elasticity monitoring of SLCT-LWCT 1:1, SLCT-LWCT 3:1, SLCT-LWCT-RIF 1:1, and SLCT-LWCT-RIF 3:1 was performed as shown in Fig. 6. The shear storage modulus (G') was given as a function of reaction time at 37°C. It was observed that all four formulations had a relatively fast onset of gelation of less than 2 min. Gelation onset times of 57 s was observed for SLCT-LWCT 1:1, SLCT-LWCT 3:1, and SLCT-LWCT-RIF 1:1, whereas SLCT-LWCT-RIF 3:1 demonstrated a gelation onset time of 117 s. The delayed gelation onset observed with SLCT-LWCT-RIF 3:1 could be due to a longer time required for the reacting PEC molecules to come into contact with each other as a result of excess phosphate anions in the system causing electrostatic repulsion and interference by RIF molecules. The fast onset of gelation may be attributed to a rapid polyelectrolyte complexation reaction between the native polymers of equal ratios with minimal interference from RIF. A progressive increase in G' for all formulations was noted over the 5-h duration with the drug-free formulations gelling at a faster rate than the drug-loaded formulations. This may be a result of the presence of more uninterrupted reaction sites available for polyelectrolyte complexation in the drug-free formulations, thus, supporting the FTIR-implication of possible RIF interference with NH^{3+} and PO^{3-} reaction sites. During the 5-h gelation period, it was noted that SLCT-LWCT 1:1 and SLCT-LWCT 3:1 reached a maximum G' of 282 Pa (± 13) and 319 Pa (± 11), respectively, while SLCT-LWCT-RIF 1:1 and SLCT-LWCT-RIF 3:1 peaked at 163 Pa (± 10) and 242 Pa (± 11), respectively. This may reflect the formation of a slightly disrupted PEC matrix and gelling formation in response to RIF loading whereas the drug-free formulations are able to maintain a more compact and continuous gelling arrangement throughout the sample matrix.

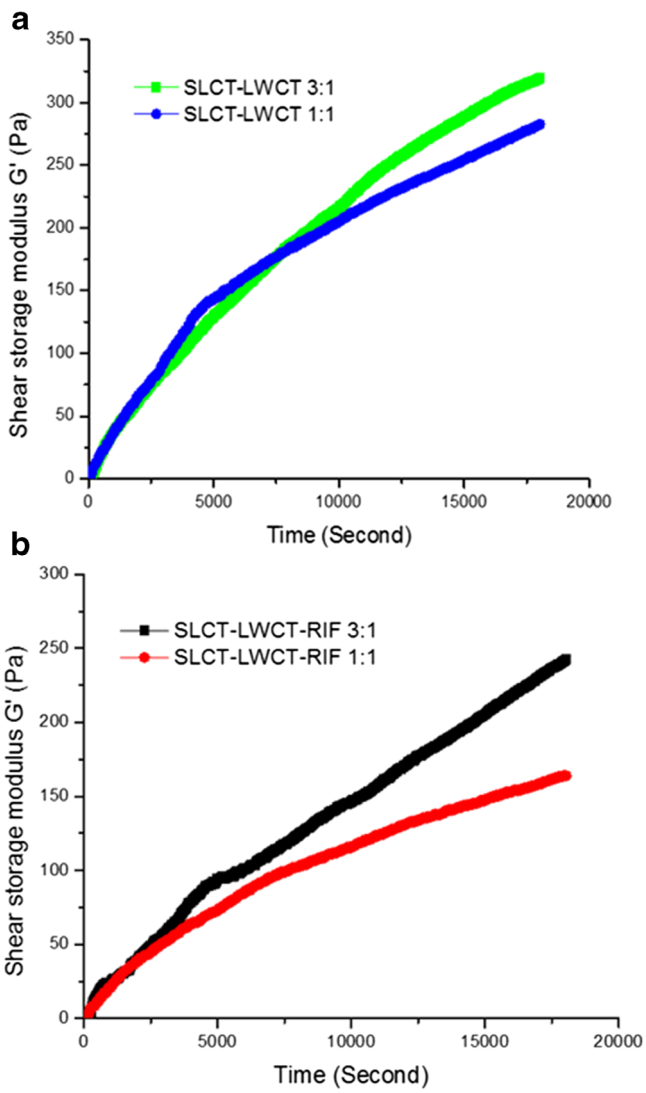

Fig. 6. Kinetic gelation plots of SLCT-LWCT 1:1, SLCT-LWCT 3:1 (**a**), SLCT-LWCT-RIF 1:1, and SLCT-LWCT-RIF 3:1 (**b**) presenting the shear storage modulus (G') (Pa) observed over a 5-h timeframe at 37°C

Textural Transitions in Response to Variations in SLCT in the RIF-loaded Lipopolysaccharide PEC Nanoparticulate Tablets

Textural profiling revealed that increased SLCT ratio in the SLCT-LWCT-RIF 3:1 formulation presented with a greater force of 12.48 N and fracture energy of 0.026 J to initiate a break in the tablet matrix whereas the 1:1 formulation achieved a break in the tablet structure at 10.48 N with a corresponding energy of 0.021 J. In addition to the PEC formation resulting from SLCT-LWCT electrostatic interactions, the increased mechanical strength of the 3:1 formulation could further be attributed to possible interactions arising from SLCT-RIF, as noted in the FTIR spectra and XRPD diffractograms. Reduced crystallinity of the lipopolysaccharide nanoparticulate system in response to increased SLCT ratios, as observed in XRPD analysis, suggests the formation of a less brittle tablet matrix imparted by a slight plasticizing effect of the soy lecithin phospholipid. In this case, a portion of energy is dissipated throughout the matrix before reaching a break in the system whereas a highly brittle matrix results in immediate breakage and cracking upon application of force due to decreased deformability of the matrix system. Likewise, the enhanced mechanical attributes obtained *via* increased SLCT in the PEC particulates correspond to the enhanced elastic (G') rheological properties of the 3:1 formulation (242 Pa) compared to the 1:1 formulation (163 Pa).

Optical Characterization and Stability of the Lipopolysaccharide PEC Particulates in Aqueous Suspension

Light scattering analysis of the synthesized drug-free (SLCT-LWCT) and drug-loaded (SLCT-LWCT-RIF) PEC particulates was performed. This analysis is based on the

principle of particle migration and particle concentration variation within the sample. The phenomena of coalescence and flocculation are detected through increases in particle size of the sample. This technique measures the migration of colloidal particles towards the (1) bottom of the sample (sedimentation), (2) top of the sample (creaming), or (3) middle portion of the sample where particle aggregation leads to increased particle size (flocculation or coalescence). The result of this particle migration is expressed as the intensity of delta backscattering (ΔBS) or transmission (T) where an increase in ΔBS at the bottom of the sample with a corresponding decrease in T at the top of the sample indicates sedimentation kinetics. The reverse is true for the case of creaming kinetics; whereas in flocculation or coalescence kinetics, a decrease in ΔBS is noted throughout all three sections of the sample (48).

The stability characteristics of RIF-loaded and RIF-free nanoparticle formulations was evaluated as a function of ΔBS and it was observed that all formulations showed some level of destabilization, as shown in Fig. 7 below. However, formulations with a higher amount of SLCT (depicted in Fig. 6b, d) displayed enhanced stability as these formulations exhibited minimal changes in ΔBS of less than 5% as compared to formulations with a lower amount of SLCT where more than 10% ΔBS was noted (Fig. 7a, c). This may be related to the emulsifying properties of SLCT (49), which assists in the reduction of surface tension between the particles and the dispersion medium, thus, keeping the PEC particulates homogenously suspended in the liquid phase. Furthermore, an increase in sample particulate size at the middle and top portions of the sample indicated by increased ΔBS of 15% and 18%, respectively, was observed in Fig. 7a of the SLCT-LWCT 1:1 complex. Similarly, The SLCT-LWCT 3:1 complex, Fig. 7c, exhibited an ΔBS of 18% and 22% at the top and middle portion of the sample, respectively. This is indicative of possible coalescence and aggregation of the suspended particles at the top and middle portions of the samples, respectively.

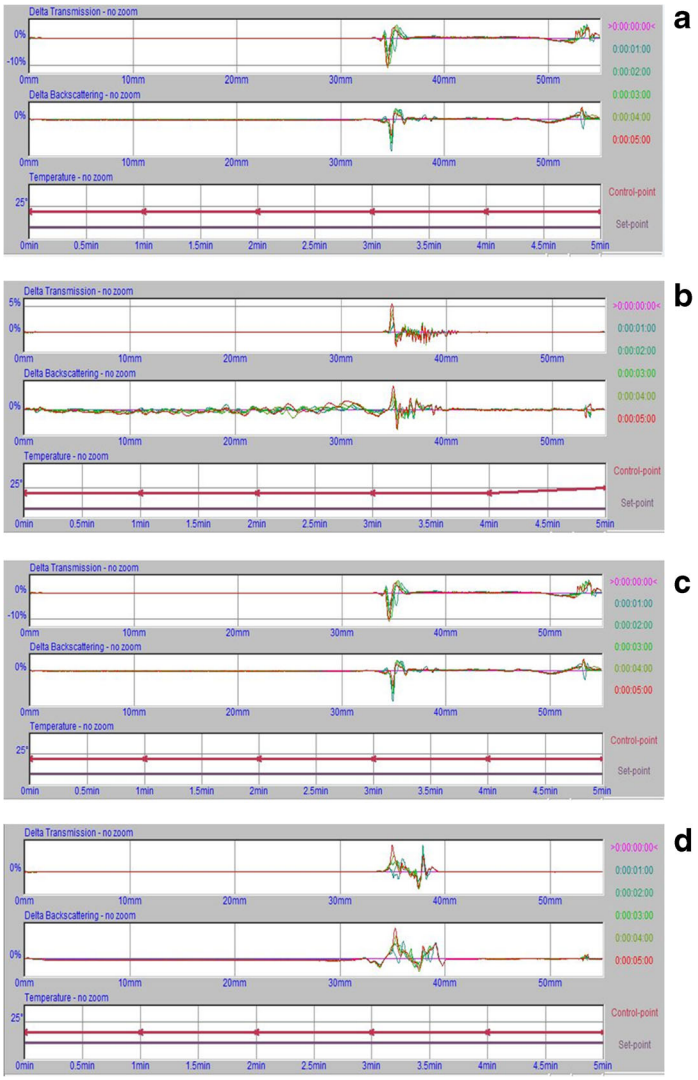

Fig. 7. Representation of the destabilization kinetics of **a** SLCT-LWCT 1:1, **b** SLCT-LWCT 3:1, **c** SLCT-LWCT-RIF 1:1, and **d** SLCT-LWCT-RIF 3:1 suspensions, indicating ΔBS and T measured at 25 ± 0.5°C for 5-min duration

The particle-migration dynamics over the 5-min analysis period revealed that the incorporation of RIF into the lipopolysaccharide nanocomplex instigated slight changes in the stability of the formulation, indicated by changes in ΔBS and T along each time interval, compared to the RIF-free systems which maintained steady ΔBS levels over the test timeframe. This is likely due to overall increased particle size and ionic charge (Table I) upon RIF encapsulation, as particularly noted with the SLCT-LWCT 3:1 formulation demonstrating a particle size change from 232.8 nm to 274.2 nm and surface charge of +22.2 mV to +30.7 mV. However, it should be noted that the addition of increased SLCT plays an important function in the maintenance of stability of the nanocomplex system which may be attributed to the increased elastic response of the system as noted from the shear storage moduli of 163 Pa (1:1) to 242 Pa (3:1) in RIF-loaded formulations and from 282 Pa to 319 Pa in RIF-free formulations, respectively. As such, SLCT-LWCT-RIF 3:1 and SLCT-LWCT 3:1 displayed the highest level of stability compared to SLCT-LWCT 1:1 and SLCT-LWCT-RIF 1:1.

Dispersion stability of nanoparticulates in suspension influences the therapeutic efficacy of the formulation in terms of drug-dose obtained post-reconstitution and before oral administration. Therefore, a solid dosage form, such as tablets, may eliminate dose-administration concerns with regard to simple use and storage of the formulation.

Evaluation and Mathematical Modeling of RIF Release from the Lipopolysaccharide PEC Particulates

The rate and quantity of drug release from a formulation plays a critical role in determining the dose administration frequency of a medicine. Thus, a formulation providing extended release kinetics reduces administration frequency, which is crucial in maintaining patient compliance in an infective disease condition such as TB. The analysis of *in vitro* drug release behavior of nanocarriers is a pertinent factor, among others (50), in determining the amount of drug available for potential absorption into the systemic circulation.

The *in vitro* release profile of RIF from the formulated lipopolysaccharide PEC particulates was investigated alongside comparator formulations (SLCT-LWCT+RIF, MSLCT-RIF+LWCT, SLCT+LWCT+RIF, and free RIF capsules). As shown in Fig. 8, it was observed that the *in situ* complexes of SLCT+LWCT+RIF (mixing of pristine polymer and drug powders), SLCT-LWCT+RIF 1:1 (*in situ* mixing of RIF with the formulated SLCT-LWCT 1:1 complex) and free RIF released 90%, 64%, and 28% of drug content, respectively, within the first 4 h, hence, exhibiting the fastest release profile. Free RIF formulation released 91% of drug content within the 24-h study period. This rapid release behavior may be attributed to a decrease or absence of intermolecular bonds between the parent polymers of the *in situ* formulation (SLCT+LWCT+RIF) and due to RIF existing in a simple dispersed form as opposed to encapsulated within the particles of the system (SLCT+LWCT+RIF, SLCT-LWCT+RIF 1:1 and free RIF). Such release profiles are considered unsuitable for sustained delivery of RIF as it potentiates frequent administration and reduced patient compliance. It was further observed that formulations of MSLCT+RIF+LWCT and SLCT-LWCT+RIF 3:1, which involved blending of RIF within melted SLCT and the SLCT-LWCT 3:1 complex, provided a cumulative drug release of 22.8% and 20.8%, respectively. In this case, the direct blending and increased ratio of SLCT in the formulation contributed to decreased drug release.

Formulations, involving authentic RIF encapsulation during the solvent injection method, SLCT-LWCT-RIF 1:1 and SLCT-LWCT-RIF 3:1 exhibited slower drug release rates with a cumulative drug release of 11.4% and 6.4%, respectively, obtained over the 24-h study period. The slower release profiles could be attributed to RIF-phospholipid electrostatic interaction and barriers imparted by the phospholipid matrix as deposition of the drug most likely occurred

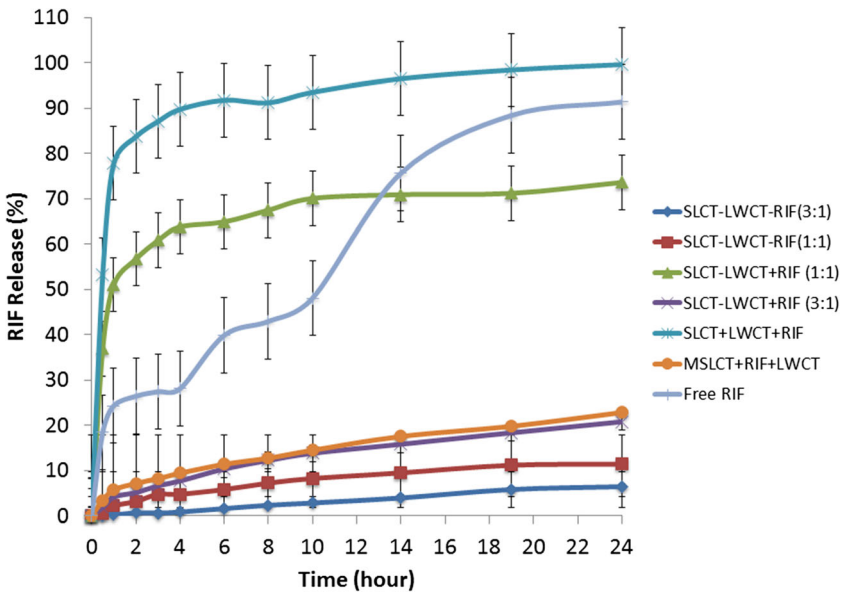

Fig. 8. *In vitro* release profile of RIF from various indicated formulations at 37°C and pH 6.8 ($n = 3$, mean ± SD)

within the lipid bilayers (21). In addition, this concept explains the low release rates observed in formulations with a higher proportion of SLCT as mentioned earlier (SLCT-LWCT-RIF 3:1 and SLCT-LWCT+RIF 3:1). Furthermore, RIF entrapped within the PEC matrix of the phospholipid-polysaccharide system contributes to slower release as passage of the drug molecules out of the system is dependent on disintegration of the PEC thus, reducing release rates. PEC particulates SLCT-LWCT-RIF 1:1 and 3:1 exhibited a significantly low cumulative drug release over a 24-h period and hence require longer time periods for complete release of loaded drug to occur. In favor of a reasonable dosing frequency and drug-interaction time, it is possible to modulate drug release rates employing enzyme-triggered drug release tactics in conjunction with adjustments in SLCT ratios to assist in rupture of the internal nanoparticle structure, thereby, conferring faster release (21, 51).

Mathematical modeling of the drug release data (as listed in Table IV) was performed to offer insight into the underlying drug release mechanisms governing the observed release profiles in response to variations in polymer ratios and tablet-preparation methods. It is noted that tablets prepared by simple mixing of the pristine polymer and drug powders (SLCT+LWCT+RIF) followed the first-order release model ($R^2 = 0.7231$) where drug release occurred *via* non-Fickian anomalous transport as indicated by the n value (> 0.45) of 0.5479 derived from the Korsmeyer-Peppas equation. Rapid disintegration of the compacted powders resulting in prompt wetting and diffusional release of RIF from this formulation contributed to the fast drug release rate of 90% within the first 4 h with complete release occurring at the end of 24 h. Formulations involving coating of RIF with melted SLCT (MSLCT+RIF+LWCT) followed the Higuchi model with $n = 0.4699$ suggesting non-Fickian diffusional release where drug release was likely dependent on the extent of hydration and dissolution of the RIF-SLCT complex, hence the slower release rate of 22.81%.

Drug release from tablets prepared from the pre-formulated PEC (SLCT-LWCT+RIF (1:1): 64% and (3:1): 20.8%) displayed a significant decrease in release rates upon increase in SLCT ratio. The faster release of the 1:1 formulation ($n = 0.2692$) profile may be attributed to the dispersion of RIF molecules within the SLCT-LWCT PEC system where RIF is dispersed within the spaces of the polymer matrix but not necessarily encapsulated and complexed to the SLCT-LWCT PEC *via* intermolecular interactions. This arrangement of RIF throughout the tablet matrix allows for rapid water penetration, hydration and swelling of the system resulting in Fickian diffusion of RIF molecules whereas the decreased release rates imparted by increased SLCT in the 3:1 formulation is possibly conferred by SLCT-RIF interactions in addition to the SLCT-LWCT complex. It is further noted that increased SLCT ratio imparts an increase in the n value suggesting a gradual shift from diffusion-based release towards non-Fickian anomalous transport ($n = 0.6013$) and erosion-controlled release (27). This is particularly evident in the tablets prepared from the lyophilized powder of the PEC particulates obtained from the concurrent incorporation of SLCT, LWCT, and RIF during the solvent injection synthesis which yielded exceptionally low drug release rates of 11.4% and 6.4% for the SLCT-LWCT-RIF 1:1 and 3:1 formulations, respectively. The release profiles transitions from Higuchi to zero-order kinetics upon increased SLCT. The increase in n value from 0.736 for the 1:1 PEC particulates to 1.2605 for the 3:1 PEC particulates implies the working of a super case II transport as the primary drug release mechanism where dissolution of the PEC-entrapped drug is time-dependent on polymer relaxation and erosion of the PEC particulates as opposed to only hydration and diffusion out of the system.

Evaluation of Hydration Dynamics Controlling Swelling and Erosion Behaviors of the RIF-loaded Lipopolysaccharide PEC Nanoparticulate Tablets

The characteristics of fluid ingress into and hydration of the SLCT-LWCT-RIF tablets are critical in understanding the drug-release mechanisms observed in terms of swelling and erosion processes which influence the drug-release kinetics. The changes in hydration and subsequent swelling and erosion of the tablet matrix at various time points, as acquired from MRI capture, is depicted in Fig. 9. The gradual grayscale color transitions from dark to light areas indicate increased water penetration and hydration of the tablet as further swelling and subsequent erosion of the matrix ensues.

The hydration sequence of the SLCT-LWCT-RIF 1:1 formulation, depicted in Fig. 9a, shows immediate disintegration and dissolution of the tablet matrix, into the surrounding media, occurring from the surface towards the core of the system with little or no presence of a defined swollen

Table IV. Mathematical Modeling for RIF Release Kinetics

Formulation	Zero-order	First-order	Higuchi	Hixson-Crowell	Korsmeyer-Peppas		Best-fit model
	R^2	R^2	R^2	R^2	R^2	n	
SLCT+LWCT+RIF	0.5259	0.7231	0.677	0.6581	1	0.5479	First-order
MSLCT+RIF+LWCT	0.9398	0.9471	0.9879	0.9447	0.9908	0.4699	Higuchi
SLCT-LWCT+RIF 1:1	0.6942	0.7741	0.8306	0.748	0.9234	0.2692	Higuchi
SLCT-LWCT+RIF 3:1	0.9723	0.9771	0.988	0.9755	0.9794	0.6013	Higuchi
SLCT-LWCT-RIF 1:1	0.9032	0.9089	0.9678	0.907	0.89	0.736	Higuchi
SLCT-LWCT-RIF 3:1	0.9681	0.9675	0.904	0.9677	0.9811	1.2605	Zero-order

SLCT soy lecithin, *LWCT* low-molecular-weight chitosan, *RIF* rifampicin, *MSLCT in situ* complex of SLCT-coated RIF and pristine LWCT

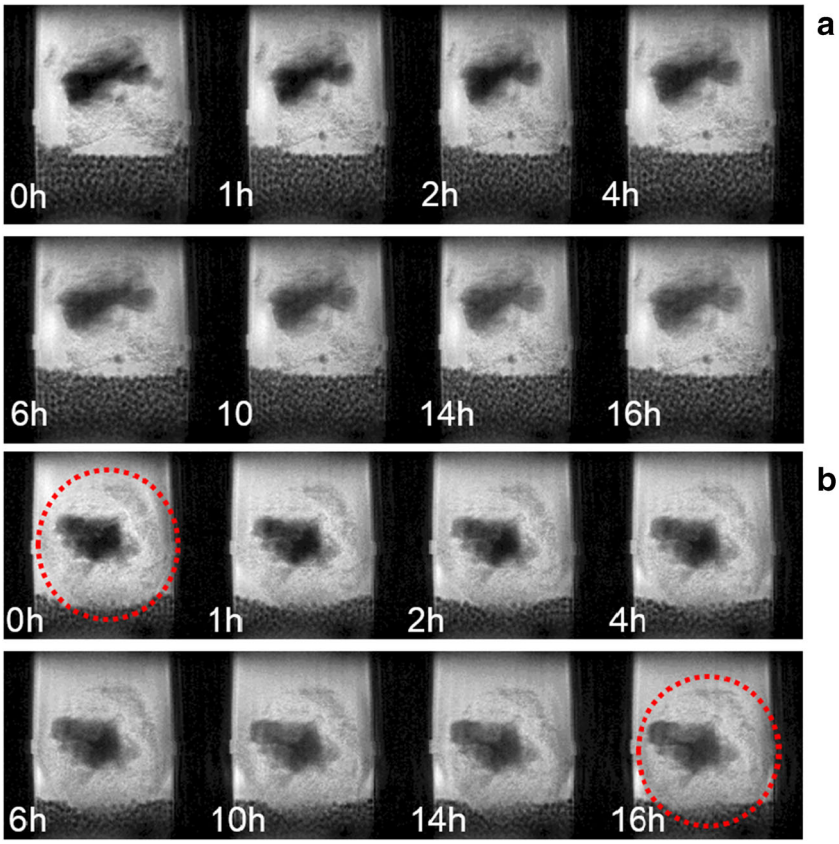

Fig. 9. MRI acquisition illustrating the progression of fluid ingress and hydration of nanoparticulate tablets formulated from **a** SLCT-LWCT-RIF 1:1 and **b** SLCT-LWCT-RIF 3:1 (formation of a distinct swelling zone encircled in red) over a time period of 16 h

interface. This correlates to the drug-release kinetics obtained which indicated a slightly faster release pattern (11.4% cumulative release) controlled *via* a combination of diffusion and erosion processes (non-Fickian anomalous transport). In contrast, the hydration dynamics of the SLCT-LWCT-RIF 3:1 formulation, depicted in Fig. 9b, shows the formation of a distinctive swollen zone (highlighted in red) surrounding an inner core of unhydrated matter. This gelled interface further retards the diffusion of RIF molecules out of the matrix (where RIF remains entrapped for a longer time in the gelled state of this layer) thereby presenting with decreased drug release rates of 6.4% cumulative release. In this case, the predominant mechanism of super case II transport encompasses time-dependent PEC matrix hydration and subsequent swelling followed by polymer chain relaxation and erosion of the gelled region thereby following zero-order drug-release kinetics where the matrix system does not disintegrate but maintains its bulk in a swollen or gelled state.

Ex vivo Evaluation of RIF Permeation Across Porcine Intestinal Tissue from the Lipopolysaccharide PEC Particulates

The rate and extent of drug permeation through the intestinal barrier is governed by several factors, such as physiological, biological, and anatomical properties of the tissue and physicochemical properties of the drug and dosage form (52), which ultimately influence drug solubility and bioavailability at the targeted delivery site. The Biopharmaceutics Classification System (BCS) has categorized RIF as a Class II drug (high permeability, low solubility); however, several studies have queried this classification and prior research has established RIF as a drug of low permeability and low solubility (BSC Class IV) (53–55).

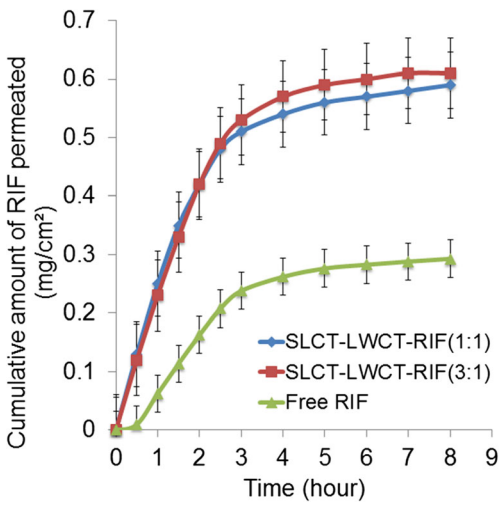

Fig. 10. Cumulative RIF permeation across pig intestinal tissue from SLCT-LWCT-RIF 1:1, SLCT-LWCT-RIF 3:1, and free RIF formulations (37°C)

Table V. Cumulative Amount of RIF Permeated (*M*), Flux Value (*J*), and Permeability (*P*) of RIF from SLCT-LWCT-RIF 1:1, SLCT-LWCT-RIF 3:1, and Free RIF Formulations After 8-h Exposure Time

Formulation	*M* (mg)	*J* (10^{-3} mg/cm^2/min)	*P* (10^{-6} cm/s)
SLCT-LWCT 1:1	1.037	1.22	21.89
SLCT-LWCT 3:1	1.079	1.27	22.85
Free RIF	0.518	0.61	10.53

RIF rifampicin, *SLCT* soy lecithin, *LWCT* low-molecular-weight chitosan

The permeability kinetics of RIF from the lipopolysaccharide PEC particulate formulations (SLCT-LWCT-RIF 1:1 and SLCT-LWCT-RIF 3:1) were evaluated alongside capsulated free RIF, as represented in Fig. 10 and Table V. It was revealed that RIF release from SLCT-LWCT-RIF 1:1 and SLCT-LWCT-RIF 3:1 significantly demonstrated enhanced permeability over the 8-h study period as compared to that of free RIF, with an average flux of 1.22×10^{-3} mg/cm^{-2}/min^{-}, 1.27×10^{-3} mg/cm$^{-2/}$min, and 0.61×10^{-3} mg/cm^{-2}/min^{-1}, respectively. Furthermore, the effective permeability (P) of RIF was found to be 21.89×10^{-6} cm/s, 22.85×10^{-6} cm/s, and 10.53×10^{-6} cm/s in SLCT-LWCT-RIF 1:1, SLCT-LWCT-RIF 3:1, and free RIF, respectively. The high permeability of RIF from the lipopolysaccharide PEC particulate formulations may be attributed to an amphiphilic property imparted by the PEComplexation which improved its interaction with the phospholipid bilayer of the intestinal membrane thereby contributing to a high migration of RIF molecules from the donor to the receptor chambers (56). The permeation of RIF from the PEC particulate formulations may occur *via* molecular transport across the membrane through the transcellular routes that often favors compounds of amphiphilic nature (57). Furthermore, as per FTIR analysis in Fig. 3a, the spontaneous chelation of RIF to LWCT and its encapsulation within the lipopolysaccharide PEC system could confer the drug molecule with increased solubility and hence, improved permeation upon dissolution. Compared to free RIF, the lipopolysaccharide PEC particulates proved as efficient nanocarriers of drug. The data obtained, showed no significant change in the permeability profile of RIF with increase in the SLCT-LWCT mass ratio from LWCT-RIF 1:1 to SLCT-LWCT-RIF 3:1.

CONCLUSION

Conventional RIF delivery systems have been identified with several drawbacks, which include but are not limited to, poor bioavailability and sustained-release properties. The lipopolysaccharide PEC particulates synthesized by the solvent injection technique, reported in the present study, has shown efficacy in promoting a sustained-release profile with reduced drug release rates imparted by molecular interaction and subsequent encapsulation of RIF within a PEC system where polymer-polymer and polymer-drug interactions are likely, as confirmed by FTIR and DSC. MRI analysis further revealed and confirmed the drug release mechanism which involved entrapment of RIF within a swollen gel interface. A series of comparator formulations further demonstrated the importance of the solvent injection technique in acquiring a successfully formulated SLCT-LWCT-RIF complex wherein drug is bound within the PEC complex as opposed to dispersed around the PEC matrix. Increase in amorphous regions, indicated by XRD, suggests an improved solubility profile of the encapsulated RIF thereby, potentially improving bioavailability. The concentration-dependent incorporation of SLCT provides a means for adjusting particle-suspension stability and drug release rates while conferring enhanced viscoelasticity and deformability of the system. Furthermore, *ex vivo* permeation studies revealed that RIF permeability can be improved by incorporating it within the PEC nanostructure of SLCT-LWCT, hence, offering a promising strategy for improving bioavailability. Despite the results obtained, comprehensive *in vivo* analysis is required to evaluate the therapeutic efficacy of the lipopolysaccharide PEC particulates in delivering adequate quantities of RIF *via* the oral delivery route with regard to bioavailability.

ACKNOWLEDGMENTS

This work was supported by the National Research Foundation (NRF) of South Africa.

COMPLIANCE WITH ETHICAL STANDARDS

Disclosure The authors declare that they have no conflicts of interest.

Publisher's Note Springer Nature remains neutral with regard to jurisdictional claims in published maps and institutional affiliations.

REFERENCES

1. Costa A, Pinheiro M, Magalhães J, Ribeiro R, Seabra V, Reis S, et al. The formulation of nanomedicines for treating tuberculosis. Adv Drug Deliv Rev. 2016;102:102–15. https://doi.org/10.1016/j.addr.2016.04.012.
2. Rappuoli R, Aderem A. A 2020 vision for vaccines against HIV tuberculosis and malaria. Nature. 2011;473(7348):463–9. https://doi.org/10.1038/nature10124.
3. Sosnik A, Carcaboso ÁM, Glisoni RJ, Moretton MA, Chiappetta DA. New old challenges in tuberculosis: potentially effective nanotechnologies in drug delivery ☆. Adv Drug Deliv Rev. 2010;62(4–5):547–59. https://doi.org/10.1016/j.addr.2009.11.023.
4. Pinheiro M, Reis S. Liposomes as drug delivery systems for the treatment of TB. Review. Nanomedicine (Lond). 2011;6:1413–28.
5. Bachhav SS, Dighe VD, Kotak D, Devarajan PV. Erratum to 'Rifampicin Lipid-Polymer hybrid nanoparticles (LIPOMER) for enhanced Peyer's patch uptake' (International Journal of Pharmaceutics (2017) 532 (612–622) (S0378517317309067) (10.1016/j.ijpharm.2017.09.040)). Int J Pharm. 2017;534(1–2):387–90. https://doi.org/10.1016/j.ijpharm.2017.09.040.
6. Petkar KC, Chavhan S, Kunda N, Saleem I, Somavarapu S, Taylor KMG, et al. Development of novel octanoyl chitosan nanoparticles for improved rifampicin pulmonary delivery: optimization by factorial design. AAPS PharmSciTech. 2018;19(4):1758–72. https://doi.org/10.1208/s12249-018-0972-9.
7. Patil J, Devi VK, Devi K, Sarasija S. A novel approach for lung delivery of rifampicin-loaded liposomes in dry powder form for the treatment of tuberculosis. Lung India. 2015;32(4):331

Available from: http://www.lungindia.com/text.asp?2015/32/4/331/159559. Accessed 19 Aug 2018.
8. El-ridy MS, Mostafa DM, Shehab A, Nasr EA, El-alim SA. Biological evaluation of pyrazinamide liposomes for treatment of Mycobacterium tuberculosis. Int J Pharm. 2007;330:82–8.
9. Devi N, Maji TK. Preparation and evaluation of gelatin/sodium carboxymethyl cellulose polyelectrolyte complex microparticles for controlled delivery of isoniazid. AAPS PharmSciTech. 2009;10(4):1412–9. https://doi.org/10.1208/s12249-009-9344-9.
10. Singh C, Koduri LVSK, Bhatt TD, Jhamb SS, Mishra V, Gill MS, et al. In vitro-in vivo evaluation of novel co-spray dried rifampicin phospholipid lipospheres for oral delivery. AAPS PharmSciTech. 2017;18(1):138–46. https://doi.org/10.1208/s12249-016-0491-5.
11. Ohashi K, Kabasawa T, Ozeki T, Okada H. One-step preparation of rifampicin/poly (lactic-co-glycolic acid) nanoparticle-containing mannitol microspheres using a four-fluid nozzle spray drier for inhalation therapy of tuberculosis. J Control Release. 2009;135(1):19–24. https://doi.org/10.1016/j.jconrel.2008.11.027.
12. Esmaeili F, Hosseini-nasr M, Rad-malekshahi M. Preparation and antibacterial activity evaluation of rifampicin-loaded poly lactide-co-glycolide nanoparticles. Nanomedicine. 2007;3:161–7.
13. Costa A, Sarmento B, Seabra V. European journal of pharmaceutical sciences mannose-functionalized solid lipid nanoparticles are effective in targeting alveolar macrophages. Eur J Pharm Sci. 2018;114(October 2017):103–13. https://doi.org/10.1016/j.ejps.2017.12.006.
14. Amarnath R, Munusamy MA, Kumar K, Rajan M. Targeted delivery of rifampicin to tuberculosis-infected macrophages: design, in-vitro, and in-vivo performance of rifampicin-loaded poly (ester amide) s nanocarriers. Int J Pharm. 2016;513(1–2):628–35. https://doi.org/10.1016/j.ijpharm.2016.09.080.
15. Rawal T, Mishra N, Jha A, Bhatt A, Tyagi RK, Panchal S, et al. Chitosan nanoparticles of gamma-Oryzanol: formulation, optimization, and in vivo evaluation of anti-hyperlipidemic activity. AAPS PharmSciTech. 2018;19(4):1894–907 Available from: http://www.ncbi.nlm.nih.gov/pubmed/29663289. Accessed 19 Aug 2018.
16. Nagpal K, Singh SK, Mishra DN. Chitosan nanoparticles: a promising system in novel drug delivery. Chem Pharm Bull (Tokyo). 2010;58(11):1423–30 Available from: https://www.jstage.jst.go.jp/article/cpb/58/11/58_11_1423/_article. Accessed 20 Aug 2018
17. Patidar A, Thakur DS, Kumar P, Verma J. A review on novel lipid based nanocarriers. Int J Pharm and Pharm Sci. 2010;2(4)30–35. Available from: https://innovareacademics.in/journal/ijpps/Vol2Issue4/806.pdf.
18. Salomon C, Goycoolea FM, Moerschbacher B. Recent trends in the development of chitosan-based drug delivery systems. AAPS PharmSciTech. 2017;18(4):933–5. https://doi.org/10.1208/s12249-017-0764-7.
19. Bhise KS, Dhumal RS, Chauhan B, Paradkar A, Kadam SS. Effect of oppositely charged polymer and dissolution medium on swelling, erosion, and drug release from chitosan matrices. AAPS PharmSciTech. 2007;8(2):Article 44.
20. Bawa P, Pillay V, Choonara YE, Claire L, Methaius V, Ndesendo K, et al. Research article a composite polyelectrolytic matrix for controlled oral drug delivery. 2011;12(1)227–238. https://doi.org/10.1208/s12249-010-9576-8.
21. Barbieri S, Sonvico F, Como C, Colombo G, Zani F, Buttini F, et al. Lecithin/chitosan controlled release nanopreparations of tamoxifen citrate: loading, enzyme-trigger release and cell uptake. J Control Release. 2013;167(3):276–83. https://doi.org/10.1016/j.jconrel.2013.02.009.
22. Pepic I, Hafner A, Lovric J. Lecithin/chitosan nanoparticles for transdermal delivery of melatonin. J Microencapsul. 2011;28(8):807–15.
23. Al-Remawi M, Elsayed A, Maghrabi I, Hamaidi M, Jaber N. Chitosan/lecithin liposomal nanovesicles as an oral insulin delivery system. Pharm Dev Technol. 2017;22(3):390–8.
24. Sahoo D, Sahoo S, Mohanty P, Sasmal S, Nayak PL. Chitosan: a new versatile bio-polymer for various applications. Des Monomers Polym. 2009;12(5):377–404.
25. Siyawamwaya M, Choonara YE, Bijukumar D, Kumar P, Du Toit LC, Pillay V. A review: overview of novel polyelectrolyte complexes as prospective drug bioavailability enhancers. Int J Polym Mater Polym Biomater. 2015;64(18):955–68.
26. Heinen C, Reuss S, Saaler-Reinhardt S, Langguth P. Mechanistic basis for unexpected bioavailability enhancement of polyelectrolyte complexes incorporating BCS class III drugs and carrageenans. Eur J Pharm Biopharm. 2013;85(1):26–33. https://doi.org/10.1016/j.ejpb.2013.03.010.
27. Cheow WS, Hadinoto K. Self-assembled amorphous drug-polyelectrolyte nanoparticle complex with enhanced dissolution rate and saturation solubility. J Colloid Interface Sci. 2012;367(1):518–26. https://doi.org/10.1016/j.jcis.2011.10.011.
28. Sonvico F, Cagnani A, Rossi A, Motta S, Di Bari MT, Cavatorta F, et al. Formation of self-organized nanoparticles by lecithin/chitosan ionic interaction. Int J Pharm. 2006;324:67–73.
29. Pawar H, Douroumis D, Boateng JS. Colloids and surfaces B: biointerfaces preparation and optimization of PMAA–chitosan–PEG nanoparticles for oral drug delivery. Colloids Surf B Biointerfaces. 2012;90:102–8. https://doi.org/10.1016/j.colsurfb.2011.10.005.
30. Ceccaldi C, Strandman S, Hui E, Montagnon E, Schmitt C, Hadj Henni A, et al. Validation and application of a nondestructive and contactless method for rheological evaluation of biomaterials. J Biomed Mater Res B Appl Biomater. 2017;105(8):2565–73.
31. Norris DA, Sinko PJ. Effect of size, surface charge, and hydrophobicity on the translocation of polystyrene microspheres through gastrointestinal mucin. J Appl Polym Sci. 1997;63(11):1481–92.
32. Liu M, Zhang J, Shan W, Huang Y. Developments of mucus penetrating nanoparticles. Asian J Pharm Sci. 2014;10(4):275–82. https://doi.org/10.1016/j.ajps.2014.12.007.
33. Jain S, Reddy CSK, Swami R, Kushwah V. Amphotericin B loaded chitosan nanoparticles: implication of bile salt stabilization on gastrointestinal stability, permeability and oral bioavailability. AAPS PharmSciTech. 2018;(10). https://doi.org/10.1208/s12249-018-1153-6.
34. Laridi R, Kheadr EE, Benech RO, Vuillemard JC, Lacroix C, Fliss I. Liposome encapsulated nisin Z: optimization, stability and release during milk fermentation. Int Dairy J. 2003;13(4):325–36.
35. Javed I, Hussain SZ, Ullah I, Khan I, Ateeq M, Shahnaz G, et al. Synthesis, characterization and evaluation of lecithin-based nanocarriers for the enhanced pharmacological and oral pharmacokinetic profile of amphotericin B. Journal of Materials Chemistry B. 2015;3(42):8359–65. https://doi.org/10.1039/c5tb01258a.
36. Cevher E, Taha MAM, Orlu M, Araman A. Evaluation of mechanical and mucoadhesive properties of clomiphene citrate gel formulations containing carbomers and their thiolated derivatives. Drug Delivery. 2008;15(1):57–67. https://doi.org/10.1080/10717540701829234
37. Chowdary KPR, Srinivasa Rao, Y. Mucoadhesive microspheres for controlled drug delivery. Biol Pharm Bull 2004;27(11):1717–24. https://doi.org/10.1248/bpb.27.1717
38. Smart J. The basics and underlying mechanisms of mucoadhesion. Adv Drug Deliv Rev. 2005;57(11):1556–68. https://doi.org/10.1016/j.addr.2005.07.001
39. Dora CP, Kushwah V, Katiyar SS, Kumar P, Pillay V, Suresh S, et al. Improved metabolic stability and therapeutic efficacy of a novel molecular gemcitabine phospholipid complex. Int J Pharm. 2017;530(1–2):113–27. https://doi.org/10.1016/j.ijpharm.2017.07.060.
40. Date PV, Samad A, Devarajan PV. Freeze thaw: a simple approach for prediction of optimal cryoprotectant for freeze drying. AAPS PharmSciTech. 2010;11(1):304–13. https://doi.org/10.1208/s12249-010-9382-3.
41. Singh C, Bhatt TD, Gill MS, Suresh S. Novel rifampicin-phospholipid complex for tubercular therapy: synthesis, physicochemical characterization and in-vivo evaluation. Int J Pharm. 2014;460(1–2):220–7. https://doi.org/10.1016/j.ijpharm.2013.10.043.
42. Alkhader E, Billa N, Roberts CJ. Mucoadhesive chitosan-pectinate nanoparticles for the delivery of curcumin to the

colon. AAPS PharmSciTech. 2016;18(4):1009–18. https://doi.org/10.1208/s12249-016-0623-y.
43. Kumar S, Dutta PK, Koh J. International journal of biological macromolecules a physico-chemical and biological study of novel chitosan—chloroquinoline derivative for biomedical applications. Int J Biol Macromol. 2011;49(3):356–61. https://doi.org/10.1016/j.ijbiomac.2011.05.017.
44. Formariz TP, Chiavacci LA, Sarmento VH V, Franzini CM, Jr AAS-, Scarpa M V, et al. Structural changes of biocompatible neutral microemulsions stabilized by mixed surfactant containing soya phosphatidylcholine and their relationship with doxorubicin release. Colloids Surf B Biointerfaces. 2008;63:287–95. https://doi.org/10.1016/j.colsurfb.2007.12.021.
45. Cheng W, Luo Z, Li L, Fu X. Preparation and characterization of debranched-starch/phosphatidylcholine inclusion complexes. J Agric Food Chem. 2015;63(2):634–41. https://doi.org/10.1021/jf504133c.
46. Celia C, Trapasso E, Cosco D, Paolino D, Fresta M. Turbiscan lab® expert analysis of the stability of Ethosomes® and ultradeformable liposomes containing a bilayer fluidizing agent. Colloids Surf B Biointerfaces. 2009;72(1):155–60.
47. Gan LJ, Wang XY, Yang D, Zhang H, Shin JA, Hong ST, et al. Emulsifying properties of lecithin containing different fatty acids obtained by immobilized lecitase ultra-catalyzed reaction. J Am Oil Chem Soc. 2014;91(4):579–90.
48. Hörter D, Dressman JB. Influence of physicochemical properties on dissolution of drugs in the gastrointestinal tract. Adv Drug Deliv Rev. 1997;25(1):3–14.
49. Vårum KM, Myhr MM, Hjerde RJN, Smidsrød O. In vitro degradation rates of partially N-acetylated chitosans in human serum. Carbohydr Res. 1997;299(1–2):99–101. https://doi.org/10.1016/s0008-6215(96)00332-1.
50. Agoram B, Woltosz WS, Bolger MB. Predicting the impact of physiological and biochemical processes on oral drug bioavailability. Adv Drug Deliv Rev. 2001;50. S41–S67. https://doi.org/10.1016/s0169-409x(01)00179-x.
51. Eduardo J, Ballerini M, Chiann C, Nella M. Effect of pH, mucin and bovine serum on rifampicin permeability through Caco-2 cells. Biopharm Drug Dispos. 2012;323(August):316–23. https://doi.org/10.1002/bdd.1802.
52. Mariappan TT, Singh S. Positioning of rifampicin in the biopharmaceutics classification system (BCS). Clin Res Regul Aff. 2006;23(1):1–10. https://doi.org/10.1080/10601330500533990.
53. Collett A, Tanianis-hughes J, Warhurst G. Rapid induction of P-glycoprotein expression by high permeability compounds in colonic cells in vitro: a possible source of transporter mediated drug interactions. Biochem Pharmacol. 2004;68:783–90. https://doi.org/10.1016/j.bcp.2004.05.006.
54. Buckley ST, Fischer SM, Fricker G, Brandl M. European journal of pharmaceutical sciences in vitro models to evaluate the permeability of poorly soluble drug entities: challenges and perspectives. Eur J Pharm Sci. 2012;45(3):235–50. https://doi.org/10.1016/j.ejps.2011.12.007.
55. Hamalainen M, Frostell-Karlsson A. Predicting the intestinal absorption potential of hits and leads. Drug Discov Today Technol. 2004;1(4):397–405. https://doi.org/10.1016/j.ddtec.2004.09.004.
56. Danaei M, Dehghankhold M, Ataei S, Hasanzadeh Davarani F, Javanmard R, Dokhani A, et al. Impact of particle size and polydispersity index on the clinical applications of lipidic nanocarrier systems. Pharmaceutics. 2018;10(2):1–17.
57. Were LM, Bruce BD, Davidson PM, Weiss J. Size, stability, and entrapment efficiency of phospholipid nanocapsules containing polypeptide antimicrobials. J Agric Food Chem. 2003;51(27):8073–9.